Geophysical Research Letters

RESEARCH LETTER
10.1029/2020GL087715

Scaling Laws for Regional Stratification at the Top of Earth's Core

Jonathan E. Mound[1] **and Christopher J. Davies**[1]

[1]School of Earth and Environment, University of Leeds, Leeds, UK

Key Points:
- CMB heat flux heterogeneity results in regional lenses of stratified fluid at the top of the core
- We develop scaling laws for the strength and thickness of these lenses
- Extrapolations to Earth-like conditions predict lenses a few hundred kilometres thick

Supporting Information:
- Supporting Information S1

Correspondence to:
J. Mound,
J.E.Mound@leeds.ac.uk

Citation:
Mound, J. E., & Davies, C. J. (2020). Scaling laws for regional stratification at the top of earth's core. *Geophysical Research Letters*, *47*, e2020GL087715. https://doi.org/10.1029/2020GL087715

Received 27 FEB 2020
Accepted 17 JUL 2020
Accepted article online 29 JUL 2020

Abstract Seismic and geomagnetic observations have been used to argue both for and against a global stratified layer at the top of Earth's outer core. Recently, we used numerical models of turbulent thermal convection to show that imposed lateral variations in core-mantle boundary (CMB) heat flow can give rise to regional lenses of stratified fluid at the top of the core while the bulk of the core remains actively convecting. Here, we develop theoretical scaling laws to extrapolate the properties of regional stratified lenses measured in simulations to the conditions of Earth's core. We estimate that regional stratified lenses in Earth's core have thicknesses of up to a few hundred kilometres and Brunt-Väisälä frequencies of hours, consistent with independent observational constraints. The location, thickness, and strength of the stratified regions would change over geological time scales in response to the slowly evolving CMB heat flux heterogeneity imposed by mantle convection.

1. Introduction

Independent inferences from seismology (Helffrich & Kaneshima, 2010; Kaneshima, 2018; Tanaka, 2007), geomagnetism (Buffett, 2014; Buffett et al., 2016; Olson et al., 2018; Yan & Stanley, 2018), and geodynamics (Davies et al., 2015; Nimmo, 2015) have been used to suggest that a stably stratified layer exists at the top of Earth's liquid core. However, some seismic studies (Alexandrakis & Eaton, 2010; Irving et al., 2018) find that a stratified layer is not required. Additionally, concentrated patches of magnetic flux at the core-mantle boundary (CMB) (Amit, 2014) and secular variation of the total geomagnetic energy at the CMB (Huguet et al., 2018) are hard to explain without radial motions near the top of the core that are difficult to reconcile with a thick and strongly stratified global layer. Nevertheless, a variety of origin mechanisms have been proposed that could produce thermal and/or compositional stratification (e.g., Bouffard et al., 2019; Brodholt & Badro, 2017; Buffett & Seagle, 2010; Gubbins & Davies, 2013; Helffrich & Kaneshima, 2013; Landeau et al., 2016; Lister & Buffett, 1998; Pozzo et al., 2012).

Convection in the core is controlled by heat flow across the CMB. Compared to the dynamics of the relatively low-viscosity core, solid-state convection in the overlying mantle is associated with long time scales and large temperature variations, such that the core is subjected to large lateral variations in CMB heat flux (Nakagawa & Tackley, 2008; Olson et al., 2015; Stackhouse et al., 2015; Zhang & Zhong, 2011). This CMB heat flux heterogeneity would interact with, and potentially disrupt, any inherent core stratification (e.g., Christensen, 2018; Cox et al., 2019; Gibbons & Gubbins, 2000; Gubbins et al., 2015; Lister, 2004; Olson et al., 2017) and can have a significant influence on the pattern of core convection and hence the geomagnetic field (e.g., Davies et al., 2008; Glatzmaier et al., 1999; Gubbins & Gibbons, 2004; Gubbins et al., 2007; Olson et al., 2015; Olson & Christensen, 2002).

An alternative view of core stratification has recently been suggested from numerical modeling in which stratification is caused, rather than opposed, by lateral CMB heat flow variations; furthermore, the resultant stratification is found to be confined into regional lenses, rather than a global layer (Mound et al., 2019). In some cases, 1D averaging over strong and laterally extensive regional inversion lenses can produce an apparent global stratification despite there being radial motion throughout the core including its outermost regions. Regional inversion lenses are ubiquitous in our simulations; however, estimation of their expected thickness L and Brunt-Väisälä frequency N in the Earth requires extrapolation from the computationally accessible parameter regime to that characteristic of Earth's core.

Three nondimensional parameters control the dynamic behavior in our numerical model of rotating nonmagnetic convection in a spherical shell (Willis et al., 2007). The Prandtl number $Pr = \nu/\kappa$ is the ratio of

the fluid's kinematic viscosity ν and its thermal diffusivity κ. The strength of convective driving is described by the Rayleigh number $\widetilde{Ra}=\alpha g_o\beta/2\Omega\kappa$, where α is the thermal expansivity of the fluid, g_o is the gravitational acceleration on the outer boundary ($r=r_o$), Ω is the planetary rotation rate, and $\beta=r_o^2 q_{ave}/k$, where q_{ave} is the average heat flux across the outer boundary and $k=\kappa\rho C_P$ is the thermal conductivity of the fluid, with ρ and C_P the fluid density and specific heat, respectively. The importance of the fluid viscosity relative to rotation is described by the Ekman number $E=\nu/2\Omega h^2$, where $h=r_o-r_i$ is the shell thickness. We describe the amplitude of heat flux heterogeneity at the CMB using $q^\star=(q_{max}-q_{min})/q_{ave}$, where q_{max} and q_{min} are the maximum and minimum heat flux, respectively (with outward heat flux defined to be positive). Scaling analysis requires simulations spanning a sufficient region of parameter space; focusing on nonmagnetic convection to reduce computational cost enabled us to explore the influence of E, $\widetilde{Ra}$, and $q^\star$ (in all cases, we hold $Pr=1$). Lorentz forces will also play a role in the Earth's core, a point that we will return to in the discussion.

Our previous work considered two patterns of CMB heat flux heterogeneity, one derived from seismic tomography (Masters et al., 1996) and an east-west hemispheric pattern, described by a spherical harmonic pattern of degree and order 1 that could be relevant when considering the mantle flow associated with supercontinent assembly (Zhong et al., 2007). Values of $q^\star=2.3$ or 5.0 were considered for the amplitude of the CMB heat flux heterogeneity. We produced a suite of nonmagnetic rotating convection simulations covering $E=\{10^{-4},10^{-5},10^{-6}\}$, $\widetilde{Ra}$ up to several hundred times the critical value for the onset of convection.

Although our simulations approach the limit of what is computationally feasible, they remain far from the parameter regime for the Earth's core. In particular, estimates of the relevant parameters suggest that $\widetilde{Ra}$ may be far larger and E far smaller in the Earth than in our simulations (Mound et al., 2019). The value of $q^\star$ is uncertain in the Earth as it requires knowledge of both the temperature structure and thermal conductivity of the lowermost mantle and the total superadiabatic CMB heat flow; nevertheless, its value in the Earth may be an order of magnitude larger than in our simulations (Mound et al., 2019). In this work, we first establish the theory relating L and N to the underlying physical parameters of the convecting system. We then show that our simulations match this theoretical expectation, enabling us to extrapolate to parameter values plausibly representative of the Earth's core.

2. Scaling Theory

The dynamics of convection falls into qualitatively different regimes depending on what combination of forces are important and which play a subdominant or inconsequential role. Scaling laws relating emergent behaviors to the imposed control parameters differ between dynamic regimes; so, care must be taken when extrapolating simulation results to planetary conditions (e.g., Aubert et al., 2017; Gastine et al., 2016; Jones, 2015; King et al., 2013). We focus on the regime of turbulent rotating convection where Inertial, Archimedean buoyancy, and Coriolis forces all play an important role in the dynamics (the IAC balance), which holds in 34 of our previously presented simulations (Long et al., 2020; Mound & Davies, 2017).

In a fluid where density decreases with increasing radius, a fluid parcel displaced radially with be returned to its original depth by buoyancy forces with a characteristic Brunt-Väisälä frequency given by

$$N^2=-\frac{g}{\rho_0}\frac{\partial\rho}{\partial r}, \tag{1}$$

where ρ_0 is a reference density. For radial density variations arising from purely thermal effects

$$N^2=\alpha g\frac{\partial T}{\partial r}. \tag{2}$$

For our Boussinesq models with fixed-flux thermal boundary conditions, the strength of thermal stratification is approximately set by the temperature gradient associated with the value of q_{min} imposed at the CMB. We note that along some radial profiles, the maximum temperature gradient occurs some distance below the outer boundary; nevertheless, we will use $\partial T/\partial r\approx -q_{min}/k$ to estimate the maximum value of N expected in our simulations. For a simple pattern of CMB heat flux variation and our definition of $q^\star$, we expect

$$q_{ave} \approx \frac{1}{2}(q_{max} + q_{min}), \tag{3}$$

and hence

$$q_{min} \approx -q_{ave}(q^{\star} - 2)/2. \tag{4}$$

Using 2Ω as our frequency scaling leads to

$$\left(\frac{N}{2\Omega}\right) \approx \left[\frac{\alpha g_o \beta}{4\Omega^2 r_o^2}\left(\frac{q^{\star} - 2}{2}\right)\right]^{1/2}. \tag{5}$$

For the Earth, it will be the average superadiabatic heat flux q_{ave}^{+} that controls the vigor of convection; so, it is useful to recast our expression for N as

$$\left(\frac{N}{2\Omega}\right) \approx \left[\frac{\alpha g_o}{8\Omega^2 k}(q_{ptp} - 2q_{ave}^{+})\right]^{1/2}, \tag{6}$$

where $q_{ptp} = q_{max} - q_{min}$ is the peak-to-peak variation in CMB heat flux. For comparison to our simulations, it is useful to combine the physical parameters into the relevant control parameters giving an expected scaling of

$$\left(\frac{N}{2\Omega}\right) \approx \frac{h}{r_o}\left[\frac{\widetilde{Ra}E}{Pr}\left(\frac{q^{\star} - 2}{2}\right)\right]^{1/2}. \tag{7}$$

Only for sufficiently strong heat flux heterogeneity will there be regions of the CMB beneath which convection is entirely suppressed. In the Earth, this requires regions of sufficiently hot lowermost mantle such that the imposed temperature gradient is subadiabatic. This requirement enters the equations above via the need for $q^{\star} > 2$ or, equivalently, $q_{ptp} > 2q_{ave}^{+}$ in order to ensure N is a positive real number.

The vigor of convection within the core is ultimately controlled by the imposed heat flux boundary conditions. The average CMB heat flux in our simulations is sufficiently supercritical with respect to the onset of convection that the fluid interior would be effectively well mixed throughout the bulk of the shell if $q^{\star} = 0$. As a result, the radial transport of heat at depth will be primarily associated with the advective term of the temperature equation ($\mathbf{u} \cdot \nabla T$). Sufficiently close to the boundary, the imposed pattern of heat flux heterogeneity will directly influence the dynamics. Under regions where the heat extracted from the core is higher than average, stronger convective motion will be driven at the top of the core, with correspondingly larger radial heat advection. Beneath regions with progressively lower CMB heat flux, the vigor of convection at the top of the core will be correspondingly reduced and eventually suppressed entirely.

In our simulations, $q^{\star}$ is sufficiently large that a thermally stratified regional inversion lens must exist immediately beneath some of the CMB. Within a lens, heat transport is radially inward and dominated by the diffusive term of the temperature equation ($\kappa\nabla^2 T$). The more anomalous the amplitude of q_{min} in our simulations, the greater the depth over which convection is suppressed by the conductive temperature profile arising due to the CMB heat flux minimum. We define the thickness of the regional inversion lenses by finding the depth of neutral stability (time-averaged $dT/dr = 0$ in our thermally driven Boussinesq model) and expect that this point is determined via competition between the temperature profiles associated with the advective heat transport in the interior and the conductive heat transport imposed at the CMB. This suggests a scaling of the form

$$\frac{UT'}{\ell} \sim \frac{\kappa \Delta T'}{L^2}, \tag{8}$$

where U is the characteristic velocity of convection, ℓ is the characteristic length scale of convection, T' is the characteristic convective temperature fluctuation, $\Delta T'$ is the total temperature anomaly across the thickness of the lens, and L is the characteristic lens thickness. Multiplying each side by $1/h^2$ and rearranging gives

Table 1
Physical Parameters for the Earth

Quantity	Symbol	Value
Density of core fluid at CMB[a]	ρ	9,903 kg m^{-3}
Gravitational acceleration at CMB[a]	g_o	10.68 m s^{2}
Radius of CMB[a]	r_o	3.480×10^{6} m
Radius of ICB[a]	r_i	1.222×10^{6} m
Rotation rate[b]	Ω	7.292×10^{-5} s^{-1}
Specific heat[c]	C_P	715 J kg^{-1} K^{-1}
Thermal expansivity[c]	α	1.8×10^{-5} K^{-1}
Thermal conductivity[d]	k	110 W m^{-1} K^{-1}

[a]Dziewonski and Anderson (1981). [b]Aoki et al. (1982). [c]Gubbins et al. (2003). [d]Pozzo et al. (2012).

$$\frac{L^2}{h^2}\sim\frac{\ell}{h}\frac{\kappa\Delta T'/h}{UT'}. \tag{9}$$

The average advective heat flux in the interior of our models will be determined by the average imposed heat flux at the CMB; so, we expect $\rho C_P UT'\sim q_{ave}$. As noted in the discussion of the scaling for the Brunt-Väisälä frequency, the strongest inverted temperature gradient (and hence conductive heat transport) can be associated with the minimum imposed CMB heat flux such that $k\Delta T'/h\sim q_{min}$. Making use of these associations and Equations 3 and 4, we can rewrite Equation 9 as

$$\frac{L^2}{h^2}\sim\frac{\ell}{h}\left[\frac{q^\star-2}{2}\right]. \tag{10}$$

The expected scaling of ℓ will depend on which force balance describes the convective dynamics. For our simulations that sit within the IAC regime, the convective length scale is expected (Aubert et al., 2001) to scale as

$$\frac{\ell}{h}\sim E^{3/5}Pr^{-2/5}Ra_F^{1/5}, \tag{11}$$

where the flux Rayleigh number $Ra_F=\widetilde{Ra}/E$ (Mound & Davies, 2017). Therefore, we expect that the thickness of the regional inversion lenses should scale as

$$\frac{L}{h}\sim E^{1/5}Pr^{-1/5}\widetilde{Ra}^{1/10}\left[\frac{q^\star-2}{2}\right]^{1/2}. \tag{12}$$

In terms of the underlying physical parameters, this scaling becomes

$$\frac{L}{h}\sim\left[\frac{\alpha g_o r_o^2}{256\rho C_P\Omega^3h^4}\right]^{1/10}\left[q_{ave}^+\right]^{-2/5}\left[q_{ptp}-2q_{ave}^+\right]^{1/2}. \tag{13}$$

The scaling laws for N and L depend on a number of physical parameters, values of which are listed in Table 1. To compare our Boussinesq model with the Earth, it is the superadiabatic heat flow across the CMB that should be used to determine the relevant thermal forcing $\beta=Q^+/4\pi k$, a quantity that is poorly constrained with even the sign of Q^+ uncertain (Jones, 2015; Olson, 2015). Regional inversion lenses will occur only if the combination of Q^+ and q_{ptp} result in a CMB heat flux pattern that has both superadiabatic and subadiabatic regions. Based on a scaling argument for core velocity, Jones (2011) estimated $Q^+\approx$ 0.6 TW; whereas a comparison of core adiabatic heat flow estimates (Davies et al., 2015) and total CMB heat flow estimates (Nimmo, 2015) suggest values as large as $Q^+\approx3$ TW are possible. We will use both of these estimates to bound our extrapolations. Similarly, the lateral variation in heat flux, q_{ptp} should be considered relative to the average superadiabatic flux, $q_{ave}^+=Q^+/4\pi r_o^2$ when determining $q^\star$; here we adopt $q_{ptp}=$ 0.14 W/m^2 (Stackhouse et al., 2015) leading to $q^\star\approx10$ or 35 for our chosen values of Q^+.

3. Scaling Results

We have determined the thickness and maximum Brunt-Väisälä frequency for the regional inversion lenses in our simulations at the centre of the lens for the hemispheric boundary forcing and at two locations beneath the CMB for our tomographic boundary forcing. For the tomographic case, we will refer to the locations as African (0°N, 0°E) and Pacific (0°N, 180°E). We first establish that our simulations obey the expected scaling by restricting ourselves to the subset of simulations with a hemispheric pattern of CMB heat flux heterogeneity. For this set of simulations, q_{min} is located where we measure N and L for the regional inversion lens and the pattern of heat flux heterogeneity obeys the adopted geometric assumptions (Equations 3 and 4); therefore, we expect this subset of lenses should best conform to the derived scalings. In Figures 1a and

1d, we plot N and L for the hemispheric simulations against the predicted scaling; the agreement between simulations and theory is indeed excellent.

For the tomographic pattern of CMB heterogeneity, $q_{\min}$ is located beneath the south Pacific; however, a regional inversion lens may still form beneath Africa provided q_{ptp} is sufficiently large. When considering the African (Figures 1b and 1e) and Pacific (Figures 1c and 1f) regional inversion lenses in our tomographic simulations, the developed scaling laws do not fit the measurements of N and L as well as they do when considering the hemispheric pattern. For the Pacific regional inversion lens characteristics, there is a systematic offset between the $q^\star = 2.3$ and the $q^\star = 5.0$ simulations in their scalings for N and L, perhaps because we have not evaluated the lens properties directly beneath $q_{\min}$ and our geometric assumptions about q (Equations 3 and 4) do not hold as well in this case. Nevertheless, each combination of CMB heat flux pattern and lens location does follow the expected scaling and the best-fit prefactors for each lens location do a reasonable job of explaining L and N across all of our simulations falling in the IAC regime.

The scaling fits to our simulations allow us to extrapolate to the conditions relevant to the Earth's core for our two choices of Q^+ (gray symbols in Figure 1, values in Table 2). For the lower value of superadiabatic CMB heat flow (Q^+_{low}=0.6 TW, gray stars) the extrapolated L and N are somewhat larger than for Q^+_{high}=3 TW (gray squares). For the chosen tomographic boundary condition, the heat flux low under the Pacific is deeper than the low under Africa. As a result, the predicted thickness and Brunt-Väisälä frequency of the Pacific lens are always larger than the African lens, with scaling predictions of $N/2\Omega = O(1)$ and $L = O(100)$ km in all cases.

4. Discussion

The developed theoretical scalings do a good job of fitting our simulations of regional inversion lenses and allow us to extrapolate to Earth's core conditions, predicting values of L and N that are geophysically plausible. Observational constraints on L and N for a global stratification at the top of the core have been derived from both seismic and geomagnetic observations. Seismic evidence allows a layer of anomalously slow P wave speed up to 450 km thick (Kaneshima, 2018); when combined with a model for chemical enrichment (Helffrich & Kaneshima, 2010), the Brunt-Väisälä frequency is inferred to be $N/2\Omega \approx 3.5 - 7.35$. Magnetic-Archimedean-Coriolis (MAC) waves in a stable layer 130–140 km thick with $N/2\Omega \approx 0.37 - 0.42$ have been suggested to explain certain periodic variations of the magnetic field (Buffett et al., 2016). The fundamental difference in our scenario is that stratified lenses arise only under regions of anomalously low CMB heat flux and are absent where the CMB heat flux is superadiabatic. The lateral temperature difference between the stratified and unstratified regions at the top of the core will drive thermal winds within the fluid core. Such flows are seen within our simulations and, when extrapolated to the Earth, suggest a vertical velocity gradient ($\partial u/\partial z$) on the order of 10^{-5} (m/s)/m (Mound et al., 2019). At depths on the order of 100 m, this corresponds to flow speeds on the order of 1 mm/s, compatible with those inferred from observations of magnetic secular variation for flow at the top of the free stream (e.g., Lesur et al., 2015).

The smaller the total superadiabatic heat flow across the CMB, the broader, stronger, and thicker the regional inversion lenses are expected to be. Ascertaining the existence and extent of regional inversion lenses at the top of the core would, therefore, provide constraints on the values of Q^+ and q_{ptp} and hence the thermal state of the lowermost mantle. As the pattern and strength of CMB heat flux heterogeneity evolves over geological time in response to ongoing mantle convection, the predicted locations, thicknesses, and strengths of regional inversion lenses would similarly evolve in response.

If a mechanism of chemical stratification is also active within the core, then this additional stabilizing contribution might enable regional inversion lenses to form for smaller values of $q^\star$ or promote thicker and stronger lenses. A global stratified layer might even result despite the CMB heat flux heterogeneity, provided that the process of light element enrichment at the top of the core is sufficiently strong to shut down convection beneath regions of superadiabatic CMB heat flow. Determining whether any such mechanism is active in Earth's core and its influence on regional inversion requires additional numerical and theoretical investigation beyond the scope of this study.

Extrapolation of regional inversion lens thickness to the Earth requires understanding of the appropriate force balance, both for the Earth and the given suite of simulations. For a given convecting system, the

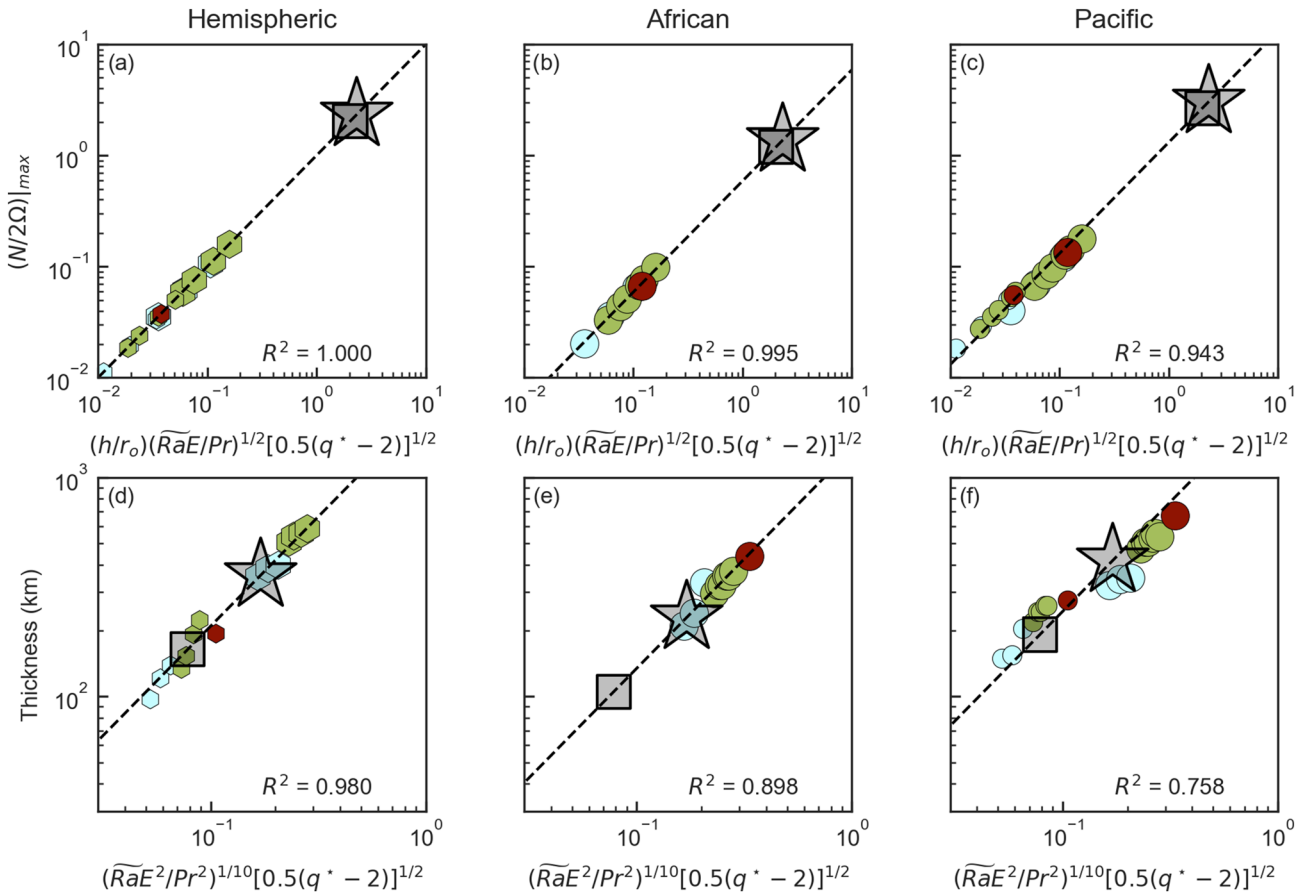

Figure 1. Scaling of the Hemispheric (a,d), African (b,e), and Pacific (c,f) regional inversion lenses in our simulations. Maximum Brunt-Väisälä frequency (a–c) and thickness (d–f) from the simulations (colored symbols) are plotted against the theoretical scaling. Colors of the filled symbols indicate $E=\{10^{-6},10^{-5},10^{-4}\}$ (light blue, olive, brick), size indicates $q^\star=\{2.3,5\}$ (small, large), and shape indicates tomographic (circles) or hemispheric (hexagons) patterns of CMB heat flux heterogeneity. The dashed lines and R^2 values are based on the best-fit prefactors for each case and the exponents predicted by our theory. These fits are used to extrapolate to the Earth for Q^+_{low}=0.6 TW (star) or Q^+_{high}=3 TW (square).

dominant force balance will depend on its physical properties and boundary conditions and can differ between boundary layers and the interior and with the length-scale considered (e.g., Aubert, 2019; Aurnou & King, 2017; Gastine et al., 2016; Grossmann & Lohse, 2000; Schwaiger et al., 2019). The goodness of our fits (Figure 1) and previous analysis (Long et al., 2020; Mound & Davies, 2017) indicate that the IAC balance holds in the bulk of the fluid interior for the selected simulations. We have run additional simulations (see, Mound & Davies, 2017) that do not fall in the IAC regime. For insufficiently supercritical $\widetilde{Ra}$, the simulations sit within the weakly nonlinear regime with relatively sluggish convection that may not fill the spherical shell. For sufficiently large forcing, the rotational constraint on convection starts to break down and the simulations sit within the transitional regime between rapidly rotating and nonrotating convection. Although thick regional inversion lenses do form in simulations outside the IAC regime, they do not follow the thickness scaling developed here (Equation 13), which suggests that the global force balance does play an important role in setting L. Our simulations reach Reynolds numbers (up to $O(10^3)$) and Rossby numbers (down to $O(10^{-4})$) that are characteristic of turbulent rotating convection, as expected in Earth's core.

Table 2
Extrapolations to Earth

	Brunt-Väisälä ($N/2\Omega$)		Thickness (km)	
Case	Q^+_{Low}	Q^+_{High}	Q^+_{Low}	Q^+_{High}
East-west Hemispheric	2.33	2.04	358	164
Tomographic Africa	1.37	1.20	230	105
Tomographic Pacific	3.05	2.66	418	192

The global force balance enters into the scaling for L by determining the small length-scale associated with convection. It is possible to consider another force balance, such as one incorporating the

influence of the magnetic field on the dynamics within the Earth's core. For example, Davidson (2013) derived a scaling for ℓ assuming a MAC balance holds; substitution of his equation (12) into our Equation 10 results in

$$\frac{L}{h} \sim E^{1/9} Pr^{-1/9} \widetilde{Ra}^{1/18} \left[\frac{q^\star - 2}{2}\right]^{1/2}. \tag{14}$$

As with the scaling based on the IAC balance, this scaling depends only weakly on E, Pr, and $\widetilde{Ra}$ and hence the associated physical parameters and has the same expected scaling between L/h and $q^\star$. Therefore, we expect that if this force balance holds, a sufficiently large amplitude of CMB heat flux heterogeneity would result in the presence of thick ($O(100)$ km) regional inversion lenses at the top of the core.

Data Availability Statement

The simulation output data used to produce Figures 1 and 2 can be found in the supplementary information and can be accessed via DOI: 10.17605/OSF.IO/ES47H.

Acknowledgments
CJD is supported by a Natural Environment Research Council Independent Research Fellowship (NE/L011328/1). This work used the ARCHER UK National Supercomputing Service (http://www.archer.ac.uk) and ARC, part of the High Performance Computing facilities at the University of Leeds, UK. Figures were produced using Matplotlib (Hunter, 2007) and seaborn (Waskom et al., 2018).

References

Alexandrakis, C., & Eaton, D. W. (2010). Precise seismic-wave velocity atop Earth's core: No evidence for outer-core stratification. *Physics of the Earth and Planetary Interiors*, *180*(1–2), 59–65. https://doi.org/10.1016/j.pepi.2010.02.011

Amit, H. (2014). Can downwelling at the top of the Earth's core be detected in the geomagnetic secular variation?. *Physics of the Earth and Planetary Interiors*, *229*(C), 110–121. https://doi.org/10.1016/j.pepi.2014.01.012

Aoki, S., Guinot, B., Kaplan, G. H., Kinoshita, H., McCarthy, D. D., & Seidelmann, P. K. (1982). The new definition of universal time. *Astronomy and Astrophysics*, *105*, 359–361.

Aubert, J. (2019). Approaching Earth's core conditions in high-resolution geodynamo simulations. *Geophysical Journal International*, *219*, S137–S151. https://doi.org/10.1093/gji/ggz232

Aubert, J., Brito, D., Nataf, H.-C., Cardin, P., & Masson, J.-P. (2001). A systematic experimental study of rapidly rotating spherical convection in water and liquid gallium. *Physics of the Earth and Planetary Interiors*, *128*(1–4), 51–74. https://doi.org/10.1016/S0031-9201(01)00277-1

Aubert, J., Gastine, T., & Fournier, A. (2017). Spherical convective dynamos in the rapidly rotating asymptotic regime. *Journal of Fluid Mechanics*, *813*, 558–593. https://doi.org/10.1017/jfm.2016.789

Aurnou, J. M., & King, E. M. (2017). The cross-over to magnetostrophic convection in planetary dynamo systems. *Proceedings of the Royal Society A: Mathematical, Physical and Engineering Science*, *473*(2199), 20160731. https://doi.org/10.1098/rspa.2016.0731

Bouffard, M., Choblet, G., Labrosse, S., & Wicht, J. (2019). Chemical Convection and Stratification in the Earth's Outer Core. *Frontiers in Earth Science*, *7*, 1–19. https://doi.org/10.3389/feart.2019.00099

Brodholt, J., & Badro, J. (2017). Composition of the low seismic velocity E' layer at the top of Earth's core. *Geophysical Research Letters*, *44*, 8303–8310. https://doi.org/10.1002/2017GL074261

Buffett, B. (2014). Geomagnetic fluctuations reveal stable stratification at the top of the Earth's core. *Nature*, *507*(7493), 484–487. https://doi.org/10.1038/nature13122

Buffett, B., Knezek, N., & Holme, R. (2016). Evidence for MAC waves at the top of Earth's core and implications for variations in length of day. *Geophysical Journal International*, *204*(3), 1789–1800. https://doi.org/10.1093/gji/ggv552

Buffett, B. A., & Seagle, C. T. (2010). Stratification of the top of the core due to chemical interactions with the mantle. *Journal of Geophysical Research*, *115*, B04407. https://doi.org/10.1029/2009JB006751

Christensen, U. R. (2018). Geodynamo models with a stable layer and heterogeneous heat flow at the top of the core. *Geophysical Journal International*, *215*(2), 1338–1351. https://doi.org/10.1093/gji/ggy352

Cox, G. A., Davies, C. J., Livermore, P. W., & Singleton, J. (2019). Penetration of boundary-driven flows into a rotating spherical thermally stratified fluid. *Journal of Fluid Mechanics*, *864*, 519–553. https://doi.org/10.1017/jfm.2018.999

Davidson, P. A. (2013). Scaling laws for planetary dynamos. *Geophysical Journal International*, *195*(1), 67–74. https://doi.org/10.1093/gji/ggt167

Davies, C. J., Gubbins, D., Willis, A. P., & Jimack, P. K. (2008). Time-averaged paleomagnetic field and secular variation: Predictions from dynamo solutions based on lower mantle seismic tomography. *Physics of the Earth and Planetary Interiors*, *169*(1–4), 194–203. https://doi.org/10.1016/j.pepi.2008.07.021

Davies, C., Pozzo, M., Gubbins, D., & Alfè, D. (2015). Constraints from material properties on the dynamics and evolution of Earth's core. *Nature Geoscience*, *8*(9), 678–685. https://doi.org/10.1038/ngeo2492

Dziewonski, A. M., & Anderson, D. L. (1981). Preliminary reference Earth model. *Physics of the Earth and Planetary Interiors*, *25*(4), 297–356.

Gastine, T., Wicht, J., & Aubert, J. (2016). Scaling regimes in spherical shell rotating convection. *Journal of Fluid Mechanics*, *808*, 690–732. https://doi.org/10.1017/jfm.2016.659

Gibbons, S. J., & Gubbins, D. (2000). Convection in the Earth's core driven by lateral variations in the core–mantle boundary heat flux. *Geophysical Journal International*, *142*(2), 631–642.

Glatzmaier, G. A., Coe, R. S., Hongre, L., & Roberts, P. H. (1999). The role of the Earth's mantle in controlling the frequency of geomagnetic reversals. *Nature*, *401*(6756), 885–890.

Grossmann, S., & Lohse, D. (2000). Scaling in thermal convection: A unifying theory. *Journal of Fluid Mechanics*, *407*, 27–56. https://doi.org/10.1017/S0022112099007545

Gubbins, D., Alfè, D., Davies, C., & Pozzo, M. (2015). On core convection and the geodynamo: Effects of high electrical and thermal conductivity. *Physics of the Earth and Planetary Interiors*, *247*, 56–64. https://doi.org/10.1016/j.pepi.2015.04.002

Gubbins, D., Alfè, D., Masters, G., Price, G. D., & Gillan, M. J. (2003). Can the Earth's dynamo run on heat alone? *Geophysical Journal International*, *155*(2), 609–622.
Gubbins, D., & Davies, C. J. (2013). The stratified layer at the core-mantle boundary caused by barodiffusion of oxygen, sulphur and silicon. *Physics of the Earth and Planetary Interiors*, *215*(C), 21–28. https://doi.org/10.1016/j.pepi.2012.11.001
Gubbins, D., & Gibbons, S. J. (2004). Low Pacific Secular Variation. In J. E. T. Channell, D. V. Kent, W. Lowrie, & J. G. Meert (Eds.), *Timescales Of The Paleomagnetic Field* pp. 279–286). Washington, D. C.: American Geophysical Union. https://doi.org/10.1029/145GM21
Gubbins, D., Willis, A. P., & Sreenivasan, B. (2007). Correlation of Earth's magnetic field with lower mantle thermal and seismic structure. *Physics of the Earth and Planetary Interiors*, *162*(3–4), 256–260. https://doi.org/10.1016/j.pepi.2007.04.014
Helffrich, G., & Kaneshima, S. (2010). Outer-core compositional stratification from observed core wave speed profiles. *Nature*, *468*(7325), 807–810. https://doi.org/10.1038/nature09636
Helffrich, G., & Kaneshima, S. (2013). Causes and consequences of outer core stratification. *Physics of the Earth and Planetary Interiors*, *223*, 2–7. https://doi.org/10.1016/j.pepi.2013.07.005
Huguet, L., Amit, H., & Alboussière, T. (2018). Geomagnetic Dipole Changes and Upwelling/Downwelling at the Top of the Earth's Core. *Frontiers in Earth Science*, *6*, 1–14. https://doi.org/10.3389/feart.2018.00170
Hunter, J. D. (2007). Matplotlib: A 2D graphics environment. *Computing in Science and Engineering*, *9*(3), 90–95. https://doi.org/10.1109/MCSE.2007.55
Irving, J. C. E., Cottaar, S., & Lekić, V. (2018). Seismically determined elastic parameters for Earth's outer core. *Science Advances*, *4*, 1–9.
Jones, C. A. (2011). Planetary magnetic fields and fluid dynamos. *Annual Review of Fluid Mechanics*, *43*(1), 583–614. https://doi.org/10.1146/annurev-fluid-122109-160727
Jones, C. A. (2015). Thermal and Compositional Convection in the Outer Core. In P. Olson (Ed.), *Core Dynamics* (pp. 115–159). Amsterdam: Elsevier. https://doi.org/10.1016/B978-0-444-53802-4.00141-X
Kaneshima, S. (2018). Array analyses of SmKS waves and the stratification of Earth's outermost core. *Physics of the Earth and Planetary Interiors*, *276*, 234–246. https://doi.org/10.1016/j.pepi.2017.03.006
King, E. M., Stellmach, S., & Buffett, B. (2013). Scaling behaviour in Rayleigh–Bénard convection with and without rotation. *Journal of Fluid Mechanics*, *717*, 449–471. https://doi.org/10.1017/jfm.2012.586
Landeau, M., Olson, P., Deguen, R., & Hirsh, B. H. (2016). Core merging and stratification following giant impact. *Nature Geoscience*, *9*(10), 786–789. https://doi.org/10.1038/ngeo2808
Lesur, V., Whaler, K., & Wardinski, I. (2015). Are geomagnetic data consistent with stably stratified flow at the core-mantle boundary? *Geophysical Journal International*, *201*(2), 929–946. https://doi.org/10.1093/gji/ggv031
Lister, J. R. (2004). Thermal winds forced by inhomogeneous boundary conditions in rotating, stratified, hydromagnetic fluid. *Journal of Fluid Mechanics*, *505*, 163–178. https://doi.org/10.1017/S0022112004008298
Lister, J. R., & Buffett, B. A. (1998). Stratification of the outer core at the core-mantle boundary. *Physics of the Earth and Planetary Interiors*, *105*(1–2), 5–19. https://doi.org/10.1016/S0031-9201(97)00082-4
Long, R. S., Mound, J. E., Davies, C. J., & Tobias, S. M. (2020). Scaling behaviour in spherical shell rotating convection with fixed-flux thermal boundary conditions. *Journal of Fluid Mechanics*, *889*, 1–34. https://doi.org/10.1017/jfm.2020.67
Masters, G., Johnson, S., Laske, G., & Bolton, H. (1996). A shear-velocity model of the mantle. *Philosophical Transactions of the Royal Society A: Mathematical, Physical and Engineering Sciences*, *354*(1711), 1385–1411. https://doi.org/10.1098/rsta.1996.0054
Mound, J. E., & Davies, C. J. (2017). Heat transfer in rapidly rotating convection with heterogeneous thermal boundary conditions. *Journal of Fluid Mechanics*, *828*, 601–629. https://doi.org/10.1017/jfm.2017.539
Mound, J., Davies, C., Rost, S., & Aurnou, J. (2019). Regional stratification at the top of Earth's core due to core–mantle boundary heat flux variations. *Nature Geoscience*, *12*(7), 575–580. https://doi.org/10.1038/s41561-019-0381-z
Nakagawa, T., & Tackley, P. J. (2008). Lateral variations in CMB heat flux and deep mantle seismic velocity caused by a thermal–chemical-phase boundary layer in 3D spherical convection. *Earth and Planetary Science Letters*, *271*(1–4), 348–358. https://doi.org/10.1016/j.epsl.2008.04.013
Nimmo, F. (2015). Energetics of the Core. In P. Olson (Ed.), *Core Dynamics* (pp. 27–55). Amsterdam: Elsevier. https://doi.org/10.1016/B978-0-444-53802-4.00139-1
Olson, P. (2015). Core Dynamics: An Introduction and Overview, *Core Dynamics* (pp. 1–25): Elsevier B.V.https://doi.org/10.1016/B978-0-444-53802-4.00137-8
Olson, P., & Christensen, U. R. (2002). The time-averaged magnetic field in numerical dynamos with non-uniform boundary heat flow. *Geophysical Journal International*, *151*(3), 809–823.
Olson, P., Deguen, R., Rudolph, M. L., & Zhong, S. (2015). Core evolution driven by mantle global circulation. *Physics of the Earth and Planetary Interiors*, *243*, 44–55. https://doi.org/10.1016/j.pepi.2015.03.002
Olson, P., Landeau, M., & Reynolds, E. (2017). Dynamo tests for stratification below the core-mantle boundary. *Physics of the Earth and Planetary Interiors*, *271*, 1–18. https://doi.org/10.1016/j.pepi.2017.07.003
Olson, P., Landeau, M., & Reynolds, E. (2018). Outer Core Stratification From the High Latitude Structure of the Geomagnetic Field. *Frontiers in Earth Science*, *6*(140), 1–13. https://doi.org/10.3389/feart.2018.00140
Pozzo, M., Davies, C., Gubbins, D., & Alfè, D. (2012). Thermal and electrical conductivity of iron at Earth's core conditions. *Nature*, *485*(7398), 355–358. https://doi.org/10.1038/nature11031
Schwaiger, T., Gastine, T., & Aubert, J. (2019). Force balance in numerical geodynamo simulations: a systematic study. *Geophysical Journal International*, *219*, S101–S114. https://doi.org/10.1093/gji/ggz192
Stackhouse, S., Stixrude, L., & Karki, B. B. (2015). First-principles calculations of the lattice thermal conductivity of the lower mantle. *Earth and Planetary Science Letters*, *427*, 11–17. https://doi.org/10.1016/j.epsl.2015.06.050
Tanaka, S. (2007). Possibility of a low P-wave velocity layer in the outermost core from global SmKS waveforms. *Earth and Planetary Science Letters*, *259*(3-4), 486–499. https://doi.org/10.1016/j.epsl.2007.05.007
Waskom, M., Botvinnik, O., O'Kane, D., Hobson, P., Ostblom, J., Lukauskas, S., et al. (2018). mwaskom/seaborn: v0.9.0. https://doi.org/10.5281/zenodo.1313201
Willis, A. P., Sreenivasan, B., & Gubbins, D. (2007). Thermal core–mantle interaction: Exploring regimes for 'locked' dynamo action. *Physics of the Earth and Planetary Interiors*, *165*(1-2), 83–92. https://doi.org/10.1016/j.pepi.2007.08.002
Yan, C., & Stanley, S. (2018). Sensitivity of the Geomagnetic Octupole to a Stably Stratified Layer in the Earth's Core. *Geophysical Research Letters*, *405*, 11,005–11,011. https://doi.org/10.1029/2018GL078975

Zhang, N., & Zhong, S. (2011). Heat fluxes at the Earth's surface and core–mantle boundary since Pangea formation and their implications for the geomagnetic superchrons. *Earth and Planetary Science Letters*, *306*(3–4), 205–216. https://doi.org/10.1016/j.epsl.2011.04.001

Zhong, S., Zhang, N., Li, Z.-X., & Roberts, J. H. (2007). Supercontinent cycles, true polar wander, and very long-wavelength mantle convection. *Earth and Planetary Science Letters*, *261*(3–4), 551–564. https://doi.org/10.1016/j.epsl.2007.07.049